

Comprehensive study of high- T_c interface superconductivity

G. Logvenov¹, A. Gozar¹, V. Y. Butko², A. T. Bollinger¹, N. Bozovic³, Z. Radovic⁴,
and I. Bozovic^{1*}

¹ *Condensed Matter Physics & Material Science Department, Brookhaven National Laboratory, Upton,
NY, 11973*

² *Ioffe Physical Technical Institute, 26 Polytechnical Str., St. Petersburg 194021, Russia*

³ *Department of Mathematics San Jose State University, San Jose, California 951992 USA*

⁴ *Department of Physics, University of Belgrade, Belgrade 11000, Serbia*

**corresponding author: e-mail: bozovic@bnl.gov*

Abstract

Using ALL-MBE technique, we have synthesized different heterostructures consisting of an insulator La_2CuO_4 (I) and a metal $\text{La}_{1.55}\text{Sr}_{0.45}\text{CuO}_4$ (M) layer neither of which is superconducting by itself. The M - I bilayers were superconducting with a critical temperature $T_c \approx 30$ - 36 K. This highly robust phenomenon is confined within 1-2 nm from the interface and is primarily caused by the redistribution of doped holes across the interface. In this paper we present a comprehensive study of the interface superconductivity by a range of experimental techniques including transport measurements of superconducting properties.

1. Introduction

Functionality of interfaces between strongly correlated oxide materials has been at the focus of much research recently. A range of fascinating interface electronic phenomena – high mobility 2 D electron gas, quantum Hall effect, and interface superconductiv-

ity - have been discovered [1-4]. The electronic states at the interface are influenced by many factors including interface roughness, cation interdiffusion, strain due to mismatch in the lattice constants, structure reconstruction due to the ionic character of the crystal and polar surface termination, charge depletion/accumulation driven by the difference in chemical potentials, etc. Therefore, to understand a particular interface phenomenon one not only needs a technology to prepare oxide heterostructures of very high quality but also access to a range of experimental techniques.

In this paper we report our present understanding of the high-temperature interface superconductivity in cuprate bilayers consisting of an insulator La_2CuO_4 (LCO) and a metal $\text{La}_{1.56}\text{Sr}_{0.44}\text{CuO}_4$ (LSCO) neither of which is superconducting in isolation [4]. The main difficulty in the study of interfaces in this system, in comparison to semiconducting heterostructures and p-n junctions, is the very short characteristic screening length, l_{TF} . Indeed, in cuprates $l_{\text{TF}} \sim 1$ nm, which is comparable to the height of one unit cell (1 UC), and also to the superconducting coherence length, ξ . In addition, since LSCO is a solid solution of Sr in an LCO matrix, one can not a priori exclude the possibility of some La/Sr mixing due to diffusion across the nominal interface. The diffusion coefficient and the characteristic length of diffusion of Sr across the LSCO/LCO interface under our growth conditions are actually not known. Thus, one of the first tasks is to differentiate the effects of chemical interdiffusion from those that originate in depletion/accumulation of the mobile charge carriers near the interface.

This report is based on extensive data sets obtained by a suite of advanced techniques. Several hundred LSCO-LCO heterostructures were synthesized using a unique atomic layer-by-layer molecular beam epitaxy system (ALL-MBE) [4,5]. The crystal

structure was monitored during growth by Reflection high energy electron diffraction (RHEED), while the chemical composition of surface layer was studied using the Time-of-flight ion scattering and recoil spectroscopy (TOF-ISARS) [6]. The superconducting transport and screening properties of the films were studied by measuring the dc resistance and the mutual inductance, respectively. The microstructure of *M-I* bilayers was analyzed using a high resolution scanning transmission electron microscope (STEM) with electron energy loss spectroscopy (EELS) [4]. The profile of charge carrier density in LSCO-LCO superlattices has been determined from resonant soft X-ray scattering (RSXS) data [7]. The lattice parameters of single-phase films and of heterostructures were determined by high-resolution X-ray diffraction [8].

2. Heterostructure synthesis and *in-situ* characterization

The films reported here were synthesized using the ALL-MBE system [4,5]. We used single-crystal LaSrAlO₄ substrates polished with the (001) axis perpendicular to the surface, with a typical miscut of $< 0.1^\circ$. During growth the substrates were kept at $T_s \approx 660^\circ \pm 5^\circ\text{C}$, according to the nominal pyrometer reading. The film synthesis took place at a chamber pressure $p \approx 8 \times 10^{-6}$ Torr in an atmosphere consisting essentially of pure ozone.

The growth kinetics was controlled by source shuttering using pneumatic linear-motion actuators. The growth rate was $\sim 0.05 \text{ \AA}/\text{sec}$. The deposition rates from individual thermal effusion cells were monitored and controlled in real time using an Atomic Absorption Spectroscopy system. The absolute rates were checked before growth using a quartz crystal balance, which was calibrated by measuring the film thickness using a pro-

filometer, Rutherford backscattering, grazing-angle X-ray reflectance oscillations, and X-ray diffraction finite-thickness fringes. The quality of growth was monitored in real time by means of RHEED. In Fig. 1 (a), we show a typical RHEED pattern obtained from a smooth LSCO surface. In Fig. 1 (b), we illustrate the diffraction dynamics by plotting the diffracted intensity along the dashed line in Fig 1 (a) as a function of time, during the complete deposition of one $3xM + 3xI$ bilayer heterostructure. The RHEED intensity integrated over a small area around the specular reflection spot, shown as the rectangle in Fig 1 (a), is plotted as a function of time in Fig. 1 (c). The graph shows pronounced oscillations, with the phase dynamics reflecting the changes in surface coverage and reconstruction between the first couple of layers and the remaining ones.

The surfaces of single-phase films and heterostructures were studied by Atomic force microscopy (AFM). A typical AFM image of an LSCO-LCO bilayer is shown in Fig. 2. The rms surface roughness is about 0.4 nm, less than 0.5 UC. No secondary phase precipitates, grains, or grain boundaries are seen.

Our ALL-MBE deposition chamber is equipped with TOF-ISARS system, which is a surface-sensitive technique for *in-situ* measurements of the chemical composition [6]. It allows us to place an absolute upper limit on the amount of possible Sr diffusion along the growth direction in $M-I$ bilayers. In Fig. 3 we show the evolution of peak associated with recoiled Sr from the top surface layers as a result of elastic binary collisions with the incoming 10 keV K^+ projectiles. The parameters were tuned to maximize the surface sensitivity: we used a low incidence angle of about 15° , a low index crystallographic azimuth, (100), and monitored single-scattering events. Assuming that the integrated intensity of Sr recoil peak is proportional to its surface concentration we can put an upper limit

on the length over which Sr diffusion could provide significant doping levels to about 1 UC. This is actually an overestimate, because some contribution to TOF-ISARS spectra comes from projectiles that penetrate beyond the top atomic layer.

3. The microstructure of *M-I* bilayers

The microstructure of an *M-I* bilayer and its interfaces was analyzed using STEM-EELS. [4] An upper limit on the amount of chemical interdiffusion at the interfaces was obtained by recording the Lanthanum-M_{4,5} and oxygen-K (O-K) EELS edges. The rms interface roughness at the *M-I* interface, determined by fitting the error function to the La profile and to the mobile hole distribution, was $\sigma = 1.2 \pm 0.4$ nm, comparable to 1 UC height. This value is in good agreement with the one obtained from the TOF-ISARS data.

Contributions to the interface roughness may come from several sources: (i) diffusion of Sr ions from *M* to *I* layer; (ii) the projection of the surface roughness of the substrate, and (iii) local variations in the termination layer of the substrate, which can cause extended defects (edge dislocations) in the *M* layer which nucleate at the cuprate-substrate interface. If we neglect (ii) and (iii) and attribute the interface roughness entirely to diffusion of Sr ions from the *M* layer to the *I* layer, we can put an upper limit on the out-of-plane diffusion coefficient for Sr ions (D_{Sr}) at growth temperature, as follows. Denoting by Λ the characteristic length of the interface, we have $\Lambda \approx 1 \text{ UC} \approx (D_{\text{Sr}}t)^{1/2}$, where t is the time of our growth process. For the typical value $t \sim 2,000$ s, we get $D_{\text{Sr}} \sim 10^{-21} \text{ m}^2/\text{s}$, which is negligibly small compared to the known values for bulk diffusion in oxides [9]. This indicates that our films have low concentration of defects and imperfections that could promote massive Sr diffusion.

4. Redistribution of mobile holes across the M - I interface

At the interface of two dissimilar and electrically conductive materials with different chemical potentials, μ_1 and μ_2 , an accumulation/depletion layer is expected to form as a result of migration of mobile charge carriers (electrons or holes) from one material to the other. According to the X-ray photoemission data [10], the chemical potential in $\text{La}_{2-x}\text{Sr}_x\text{CuO}_4$ system depends on the doping level: in the overdoped regime (when Sr content $x > 0.15$), one has $d\mu/dx \sim 1.5$ eV/hole, while in the underdoped regime ($x < 0.15$) the slope is very low, $d\mu/dx < 0.2$ eV/hole. Therefore, in our M - I heterostructure the chemical potential difference between overdoped LSCO ($x = 0.44$) and insulating LCO ($x = 0$) layers is $\Delta\mu \approx 0.5$ eV. Using $\Delta\mu = end^2/2\epsilon_r\epsilon_0$ [11], where the carrier density in the M layer is $n \sim 10^{21}$ cm⁻³ and the dielectric permittivity in the I layer is $\epsilon_r = 30$ [12], we can estimate the thickness of the accumulation layer inside the LCO layer to be $d \approx 6$ Å.

A natural question is whether the interface superconductivity arises due to the effect of hole accumulation in LCO layers, or due to Sr interdiffusion alone. The RSXS technique can probe the distribution of mobile holes independently of the atomic lattice [7]. For the RSXS studies, we fabricated superlattices consisting of 15 repeats of $(2xM + 1xI)$. These films had $T_c \approx 38$ K, similar to the value in optimally doped LSCO [13] as well as in the M - I bilayers discussed in this paper. The details of the experiment and of the model used to determine the profiles of Sr atoms and of the mobile hole density are described in Ref. [7]. The main conclusion of the RSXS study was that genuine charge transfer occurs from the metallic (LSCO) layer to the insulating (LCO) layer, because the profile of hole density differs from the profile of Sr^{2+} ion distribution. The level of doping

in LCO layers is found to be close to 0.18 holes per CuO_2 plane, suggesting that the LCO layers are the locus of superconductivity in our heterostructures. This study demonstrates that charge accumulation can be achieved across transition-metal oxide interfaces despite the small screening lengths, estimated to be $\sim 6\text{-}8 \text{ \AA}$ [7].

5. Transport measurements

We have studied the superconducting transport properties of M - I , I - M , and M - S bilayers (where S stands for oxygen-doped, superconducting $\text{La}_2\text{CuO}_{4+\delta}$) by measuring the dc resistance, $R(T)$, and the mutual inductance in the transmission mode, $M(T)$, over the temperature interval from $T = 4.2 \text{ K}$ to room temperature. The typical resistive transitions for M - S , M - I and I - M bilayers are shown in Fig. 4 (c). The M - S sample is obtained by annealing an M - I bilayer in pure ozone atmosphere. The highest $T_c \approx 50 \text{ K}$ is observed in M - S bilayers; in M - I bilayers $T_c \approx 30 \text{ K}$ while the lowest $T_c \approx 15 \text{ K}$ is observed in I - M structures. (In thinner M - I bilayers we have seen somewhat higher value, $T_c \approx 36 \text{ K}$.) In Figs. 4 (a) and 4 (b), we show $R(T)$ in single-phase films of I and M , for comparison.

Several questions arise naturally: (i) why we observe different T_c in M - I and I - M bilayers? (ii) Why in M - S bilayers we see $T_c \approx 50 \text{ K}$, i.e., almost 25% larger than the highest critical temperature in our optimum doped single phase films ($T_c \approx 40 \text{ K}$)?

One of the important superconducting parameters of a superconductor, the magnetic penetration depth, λ , can be extracted from the mutual inductance measurements. In our mutual inductance set-up, the film is clamped between two axially symmetric coils, of the average radius 0.9 mm. The drive and pick-up coils have 400 and 160 turns of 46 awg Cu wire, respectively. The drive coil current was $\approx 5 \mu\text{A}$ and the data were acquired

at the frequency $\nu = 10$ kHz. The measured mutual inductance $M(T)$ is a complex number with the real and the imaginary parts corresponding to the in-phase (dissipative) and 90° out-of-phase (inductive) coupling between the coils. For the films thinner than the penetration depth ($d \ll \lambda$), the in-phase signal is proportional to λ^2/d , i.e., $M(T) \approx M_0(2\lambda^2/Rd)$, where M_0 is the mutual inductance with no film present, d is the film thickness, and R is the effective radius of the coils [15,16].

In Fig. 5 we show the real and the imaginary parts of mutual inductance of an M - I bilayer that consists of a 3 UC thick I layer on top of a 3 UC thick M -layer. From these data, we can evaluate the temperature dependence of the quantity $d/\lambda(T)^2 \sim 1/[M(T)/M_0]$ shown in the inset of Fig. 5. This quantity is proportional to the superfluid density, $n_s(T)$, in our bilayer. There is an abrupt jump in $n_s(T)$ at $T=T_c$, which can be ascribed to the Berezinski-Kosterlitz-Thouless transition [17,18]

6. Pseudomorphism – a route to T_c enhancement

The critical temperature of LSCO films strongly depends on the epitaxial strain, which is determined by the misfit between the substrate and the film lattice constants [13,19,20]. The lattice mismatch between the in-plane lattice constants of our I films and LaSrAlO_4 substrates is -1.1 %, compressive, while between M and LaSrAlO_4 it is just +0.03 %, tensile. The lattice parameters of single-phase and bilayer films were determined by high-resolution X-ray diffraction. Typical out-of plane diffraction spectra for high scanning angles are shown in Fig. 6 (a) for M - I and in Fig. 6 (b) for I - M bilayers. Since the c -axis lattice parameters of the constituent materials are fairly different, $c_0 \approx 13.15$ Å for I and $c_0 \approx 13.25$ Å for M , one would expect to see in both I - M and M - I bilay-

ers pairs of close but distinct Bragg peaks. This is illustrated in Fig. 6 (c) and Fig. 6 (d), where we show the bilayer diffraction spectra calculated assuming that the constituent layers maintained their original crystallographic structure. However, as seen from Figs. 6 (a-d), no such splitting of the Bragg peaks is observed even at high scanning angles. This means that each bilayer shows a single value of the out-of plane lattice parameter.

Adjustment of the in-plane lattice constants of the film to those of the substrate, i.e., pseudomorphic growth, is not surprising as long as the film is thinner than the critical thickness. However, as seen from Table 1, the volume of a unit cell for M is noticeably different from that of I . In view of the small compressibility, which is similar in I and M , one would therefore expect that the out-of-plane lattice constants in I and M would remain different if both were epitaxially constrained to have the same in-plane lattice constants.

One can learn more by comparing bilayers and single-phase films, see Table 1. In I - M structures $c_0 = 13.169 \text{ \AA}$, which is rather close to (within 0.1 % of) that in single-phase I films, $c_0 = 13.154 \text{ \AA}$. In M - I bilayers, it is almost identical to that in single-phase M films, $c_0 = 13.245 \text{ \AA}$. In both cases, the c_0 lattice constant and the unit cell volume of the top layer essentially adjust to those of the bottom layer. Note that the detected lattice distortions are large – e.g., in I - M bilayers the contraction of c_0 in M reaches $\sim 0.08 \text{ \AA}$, comparable to the effect of a high pressure [21,22] of about 2 GPa.

If an M - I bilayer is annealed in ozone we find that both layers expand. This is rather surprising, since this procedure is known [13] to introduce interstitial oxygen in I while leaving M essentially unaffected. Moreover, the out-of-plane lattice constant in such M - S bilayers is $c_0 = 13.289 \text{ \AA}$, which is perceptibly longer than in single-phase M films. How-

ever, again there is no apparent splitting of the Bragg peaks, and the unit-cell volumes of the two constituent layers stay equal.

The in-plane lattice constant values indicate that 20 UC thick *I* layers are relaxed, i.e., both a_0 and b_0 lattice constants are close to their bulk values, [23,24] while *M* layers of the same thickness are pseudomorphic. This can be understood by recalling that the critical thickness for *I* on LaSrAlO₄ is less than 20 lattice constants [25] while for *M* it should be significantly larger because of its much better lattice match to the substrate. On the other hand, the large adjustments of c_0 lattice constants and unit-cell volumes of the top *I* and *M* layers are surprising. We believe that the origin of this effect must be in long-range electrostatic interactions in these ionic crystals [8].

Another potentially important observation is illustrated in Fig. 7, where we show the values of T_c in our single-phase films and bilayers as a function of the value of c_0 lattice constant. Apparently, T_c scales with c_0 in a linear manner. This finding allows us to link, in a phenomenological way, the observed ‘asymmetry’ between the superconducting properties of *I-M* and *M-I* bilayers to their significant and unexpected structural differences. Likewise, the enhanced T_c in *M-S* bilayers is related to the anomalous elongation along the *c*-axis: *M-S* bilayers have the longest $c_0 = 13.289 \text{ \AA}$ and correspondingly the highest $T_c \approx 50 \text{ K}$, which is about 25-40% higher than in single-phase *S* films prepared under identical conditions. Roughly linear dependence of T_c on c_0 has already been noticed [19,20] in La_{2-x}Sr_xCuO₄ samples with different level of Sr doping; however, we wish to stress that in our case there is no Sr substitution - the lattice constants change for different reasons.

6. Conclusions

We have elucidated some of the observed peculiarities in superconducting properties of *I-M*, *M-I* and *M-S* bilayers by a combination of state-of-the-art techniques: RHEED, TOF-ISARS, RSXS and STEM-EELS. The interface superconductivity arises in a very thin layer (1-2 CuO₂ planes thick), largely due to accumulation of mobile charge carriers in the La₂CuO₄ layer. Under our growth conditions, the diffusion coefficient of Sr ions across the interface is very small, $D_{\text{Sr}} \sim 10^{-21}$ m²/s. The c_0 lattice parameter depends on the deposition sequence and is always determined by the lattice constant of the buffer layer. This structural asymmetry is the root of the difference between the transport properties of *I-M* and *M-I* bilayers. The enhancement of T_c in *M-S* bilayers can also be linked to the peculiar structure with elongated c_0 lattice constant. The volume of unit cell of the top layer adjusts to the one of the bottom layer under the influence of long-range electrostatic interactions.

Acknowledgements

The authors would like to thank O. Pelleg for useful discussions. This work was supported by the U.S. Department of Energy Project MA-509-MACA,

LITERATURE:

1. A. Ohtomo, H. Y. Hwang, *Nature* 427 (2004) 423.
2. A. Tsukazaki, A. Ohtomo, A. T. Kita, Y. Ohno, H. Ohno, M. Kawasaki, *Science* 315 (2007) 1388.
3. N. Reyren, S. Thiel, A. O Caviglia, L. F. Kourkoutis, G. Hammerl, C. Richter, C. W. Schneider, T. Kopp, A. S. Ruetschi, D. Jaccard, M. Gabay, D. A. Muller, J.-M. Triscone, J. Mannhart, *Science* 317 (2007) 1196.
4. A. Gozar, G. Logvenov, L. F. Kourkoutis, A. T. Bollinger, L. A. Gianuzzi, D. A. Muller, I. Bozovic, *Nature* 455 (2008) 782.
5. I. Bozovic, G. Logvenov, I. Belca, B. Narimbetov, I. Sveklo, *Phys. Rev. Lett.* 89 (2002) 107001.
6. A. Gozar, G. Logvenov, V. Y. Butko, I. Bozovic, *Phys. Rev B* 75 (2007) 201402.
7. S. Smadici, J. C. Lee, S. Wang, P. Abbamonte, G. Logvenov, A. Gozar, C. Deville Cavelline, I. Bozovic, *Phys. Rev. Lett* 102 (2009) 1077004.
8. V. Y. Butko, G. Logvenov, N. Bozovic, Z. Radovic, I. Bozovic, *Advanced Materials* 21 (2009) 1.
9. T. Dzhafarov, *Phys. Stat. Sol. (a)* 158 (1996) 335.
10. A. Ino, T. Mizokawa, A. Fujimori, K. Tamasaki, H. Eisaki, S. Uchida, T. Kiumra, T. Sasagawa, K. Kishio, *Phys. Rev. Lett.* 79 (1997) 2104.
11. M. S. Sze, *Physics of semiconducting devices*. John Willey & Sons, 1969.
12. C. Y. Chen, R. J. Birgeneau, M. A. Kastner, N. W. Preyer, T. Thio, *Phys. Rev B* 43 (1991) 392.

13. G. Logvenov, V. Y. Butko, C. Deville Cavelline, J. Seo, A. Gozar, I. Bozovic, *Physica B* 403 (2008) 1149.
14. P. Abbamonte, A. Rusydi, S. Smadici, G. D. Gu, G. A. Sawatzky, and D. L. Feng, *Nature Physics* 1 (2005) 155.
15. J. H. Claassen, J. E. Evetts, R. E. Somekh, Z. H. Barber, *Phys. Rev. B* 44 (1991) 9605.
16. A. B. Pippard, *Supercond. Sci. Technol.* 7 (1994) 696.
17. J. M. Kosterlitz, D. J. Thouless, *J. Phys. C* 6 (1973) 1183.
18. J. M. Kosterlitz, *J. Phys. C* 7 (1974) 1046.
19. H. Sato, M. Naito, and H. Yamamoto, *Physica C* 280 (1998) 178.
20. H. Sato, M. Naito, *Physica C* 274 (1997) 221.
21. J. Shu, J. Akella, J. Z. Liu, H. K. Mao, L. W. Finger, *Physica C* 176 (1991) 503.
22. N. C. Hyatt, J. A. Hriljac, Y. Miyazaki, I. Gameson, P. P. Edwards, *Phys. Rev. B* 65 (2002) 014507.
23. P. G. Radaelli, D. G. Hinks, A. W. Mitchell, B. A. Hunter, J. L. Wagner, B. Dabrowski, K. G. Vandervoort, H. K. Viswanathan, J. D. Jorgensen, *Phys. Rev B* 49 (1994) 4163.
24. A. Migliori, W. M. Visscher, S. E. Brown, Z. Fisk, S.-W. Cheong, B. Alten, E. T. Ahrens, K. A. Kubat-Martin, J. D. Maynard, Y. Huang, D. R. Kirk, K. A. Gillis, H. K. Kim, M. H. W. Chan, *Phys. Rev B* 41 (1990) 2098.
25. J.-P. Loquet, J. Perret, J. Fompeyrine, E. Machler, *Nature*, 394 (1998) 453.

Table 1:

<i>Sample</i>	a_0 (Å)	b_0 (Å)	c_0 (Å)	V (Å ³)
M layer	5.3137	5.3130	13.2451	373.934
M-I bilayer	5.3130	5.3122	13.2446	373.806
I layer	5.3751	5.3706	13.1545	379.742
I-M bilayer	5.3669	5.3618	13.169	378.960
S layer	5.3765	5.3745	13.2217	382.060
M-S bilayer	5.3113	5.3113	13.2890	374.894
I bulk	5.4004	5.3574	13.1555	380.662
S bulk	5.3346	5.3969	13.1646	379.019
LSAO	3.7564 (5.3123)	3.7564 (5.3123)	12.6357	178.297 (356.594)

FIGURE CAPTIONS:

Fig. 1

(a): RHEED image of an LSCO-LCO bilayer taken with the electron beam incident near the (100) direction. The distance between main streaks corresponds to the inverse of in-plane lattice constant, which in LCO and LSCO is $a_0 \approx 3.8 \text{ \AA}$.

(b): The evolution of the intensity of diffracted beam measured along the dashed line in Fig. 1 (a), as a function of time, during growth of a $(3xM + 3xI)$ bilayer.

(c): The oscillations in intensity of the specular spot in RHEED during growth of a LSCO-LCO bilayer. The intensity was integrated over the area of rectangle shown in Fig. 1 (a).

Fig. 2

(a): An atomic force microscopy (AFM) image of an LSCO-LCO bilayer. The root-mean-square roughness of the surface over $100 \mu\text{m}^2$ area is $\sim 4 \text{ \AA}$.

(b) The profile of the film surface along the line shown in Fig. 2 (a). A typical step size is $\sim 0.5 \text{ UC}$.

Fig. 3

(a): The Time-of-flight ion scattering and recoil spectra (TOF-ISARS) from the surface of an LCO thin film (black) and an LSCO film (red). The pronounced peak in the LSCO spectra corresponds to the recoil of Sr^{+2} ions.

- (b): Evolution of the normalized integrated intensity of the Sr recoil (shown in the inset) during digital deposition of LSCO on top of the LCO layer, with the increment of 0.5 UC. The dashed lines are guides for the eye.
- (c): Same as (b) for deposition of LCO on top of LSCO layer. The Sr recoil peak vanishes after deposition of 2 UC of the LCO top layer.

Fig.4

- (a): The $R(T)$ dependence in a single-phase I film.
- (b): The $R(T)$ dependence in a single-phase M film.
- (c) The $R(T)$ dependence in various bilayers. The typical values of T_c at the mid-point of the resistive transitions are $T_c \approx 15\text{K}$ in $I-M$ and $T_c \approx 30\text{K}$ in $M-I$ structures. In $M-S$ bilayers (two samples shown), $T_c \approx 50\text{K}$.

Fig. 5: Temperature dependence of the normalized mutual inductance for $M-I$ bilayer, with $T_c \approx 36\text{ K}$. The inset shows the temperature dependence of the inverse value of the mutual inductance, a quantity that is proportional to the superfluid density. M_0 is the mutual inductance measured with superconducting film removed.

Fig. 6

- (a): X-ray diffraction pattern (ω - 2θ scan) from a $M-I$ bilayer grown on LaSrAlO_4 substrate. Each constituent layer is 20 UC (26 nm) thick.
- (b): The same, for an $I-M$ bilayer.

(c): The measured diffractograms (solid lines) of an $M-I$ bilayer compared with simulation in which M and I layers were assumed to retain their bulk structure.

(d): The same as in (c), but for an $I-M$ bilayer. Experimentally, every bilayer shows a single value of the c_0 lattice constant. This is actually true for the other two lattice constants, a_0 and b_0 , as well (not shown).

Fig. 7: The dependence of the superconducting critical temperature, T_c , on the value of c_0 lattice constant in various La-Sr-Cu-O samples studied in this work. Note that the values of T_c shown for $I-M$, $M-I$ and $M-S$ structures come from very thin interfacial layers. Also note that T_c strongly depends on the hole density, which in the S layers within $M-S$ structures need not be the same as in our single-phase S films, because the c -axis expansion may affect the intake of interstitial oxygen. The dashed red line is a linear fit to the data.

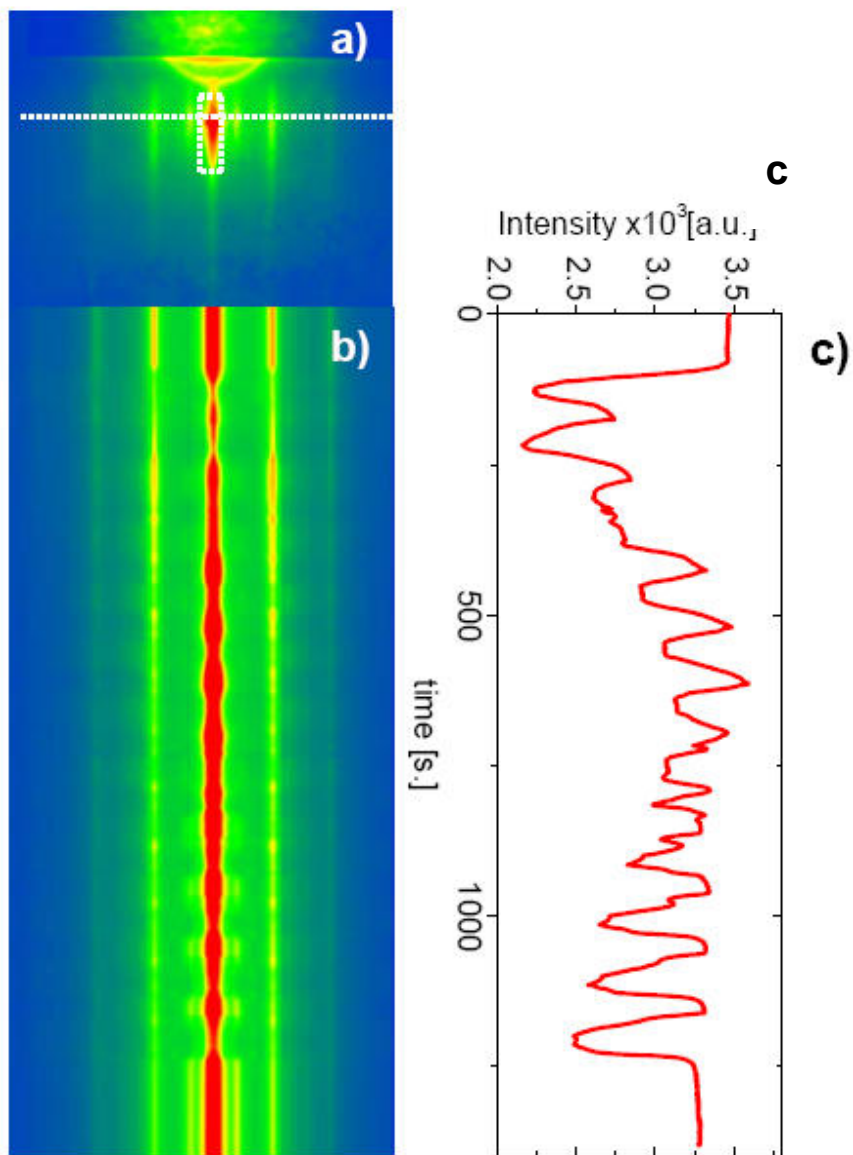


Figure 1

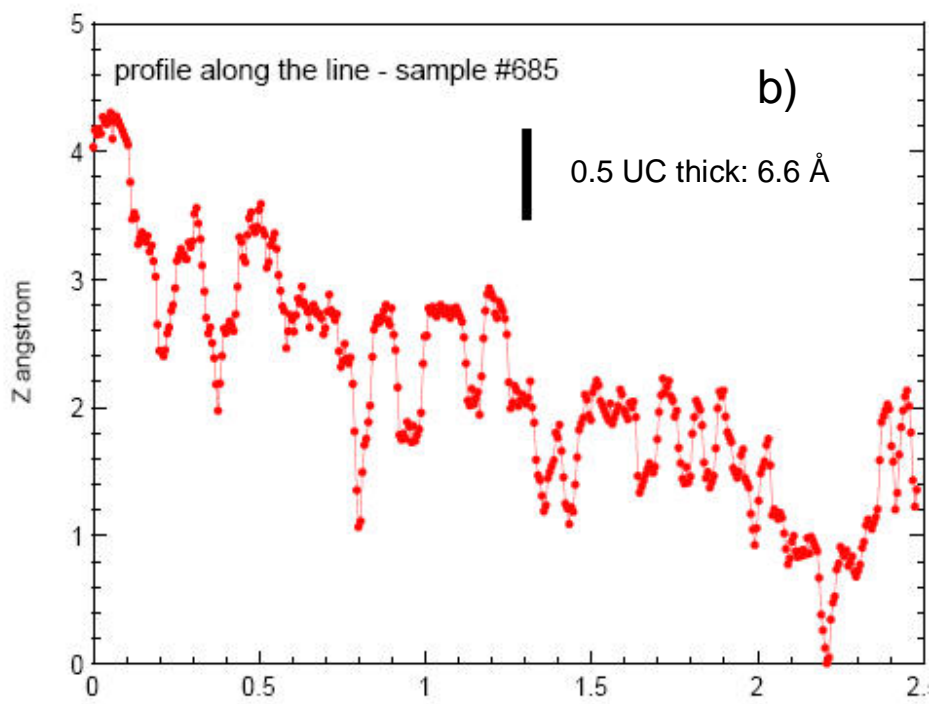
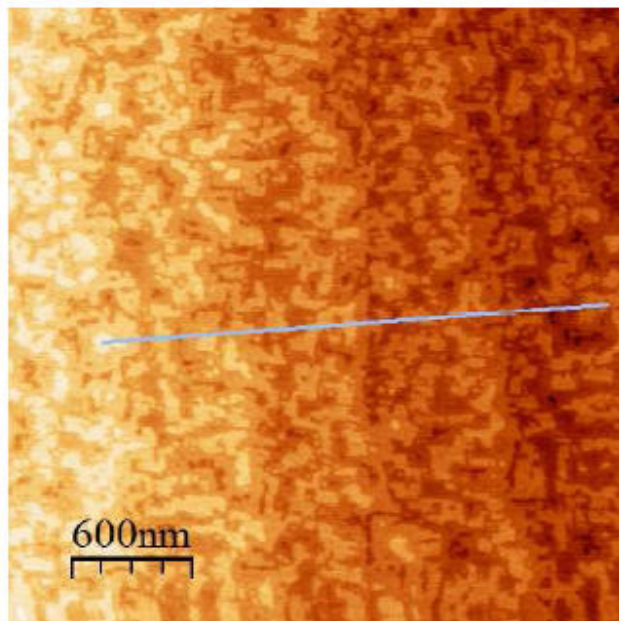


Figure 2

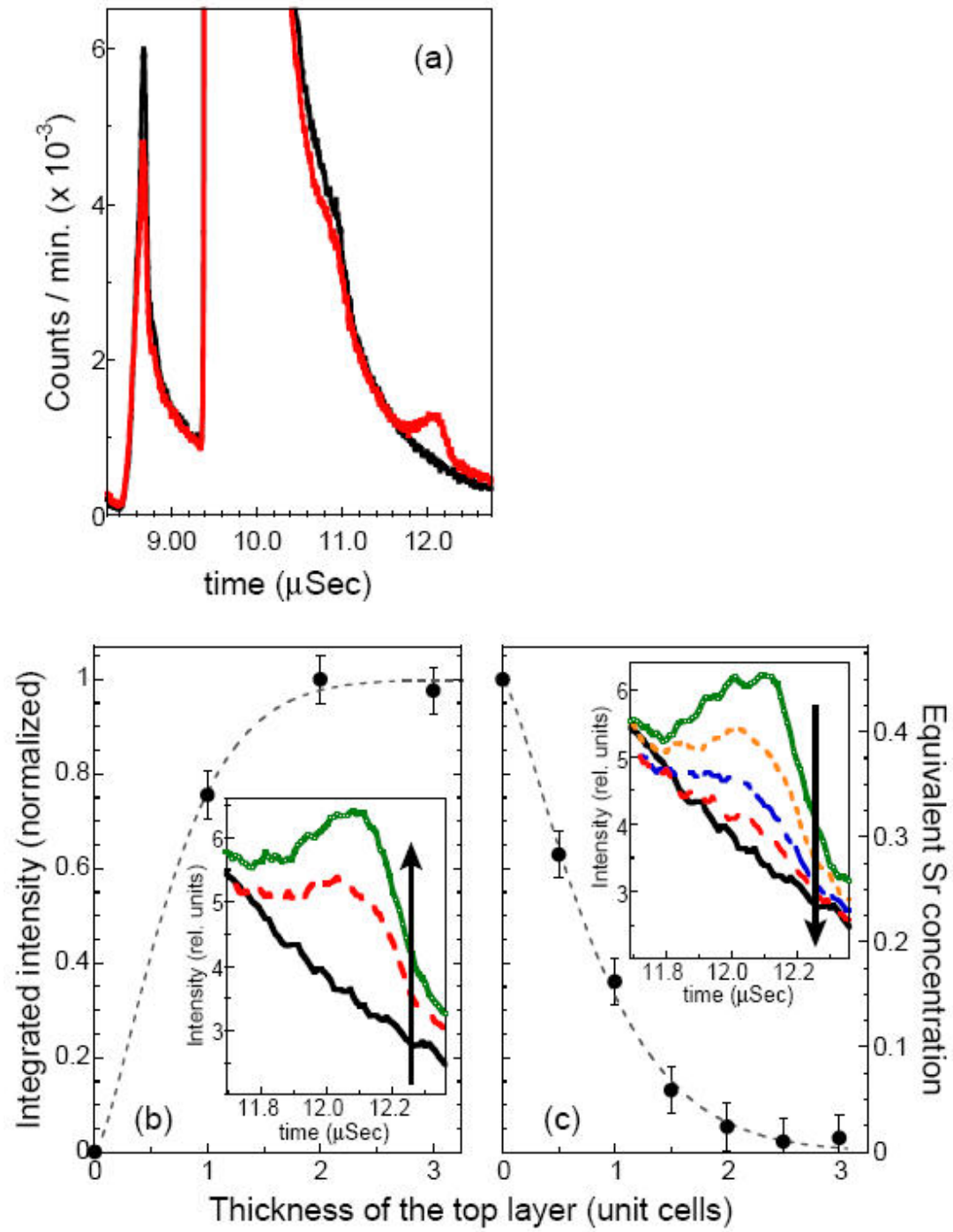


Figure 3

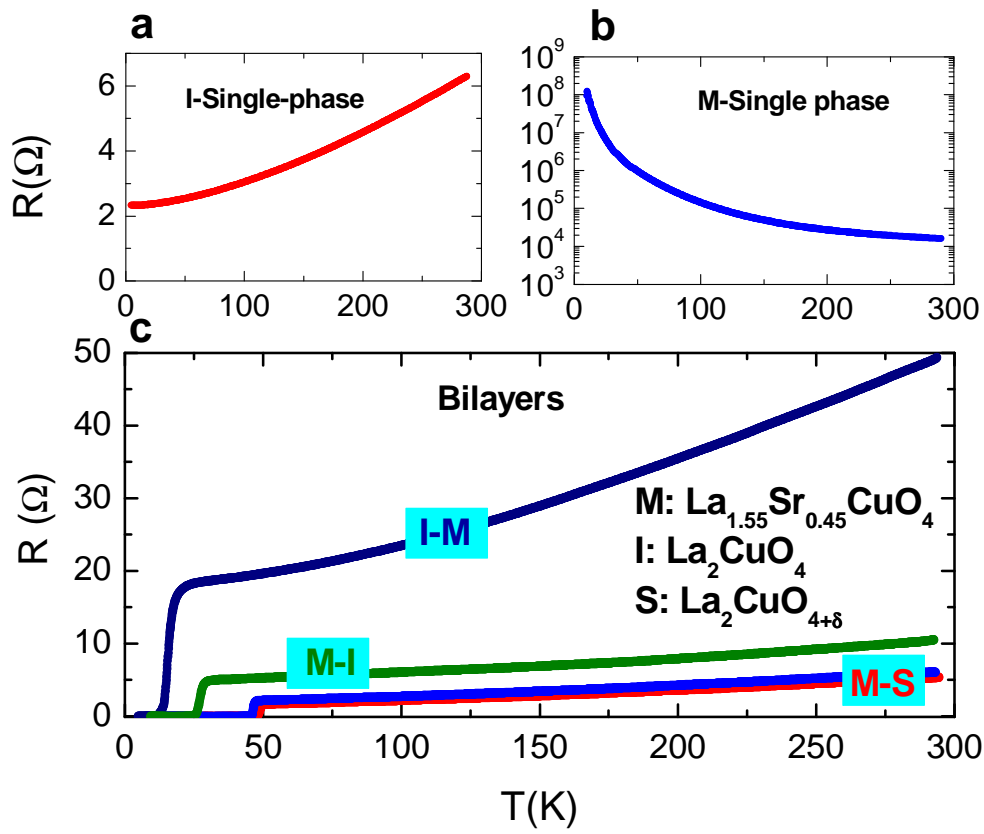


Figure 4

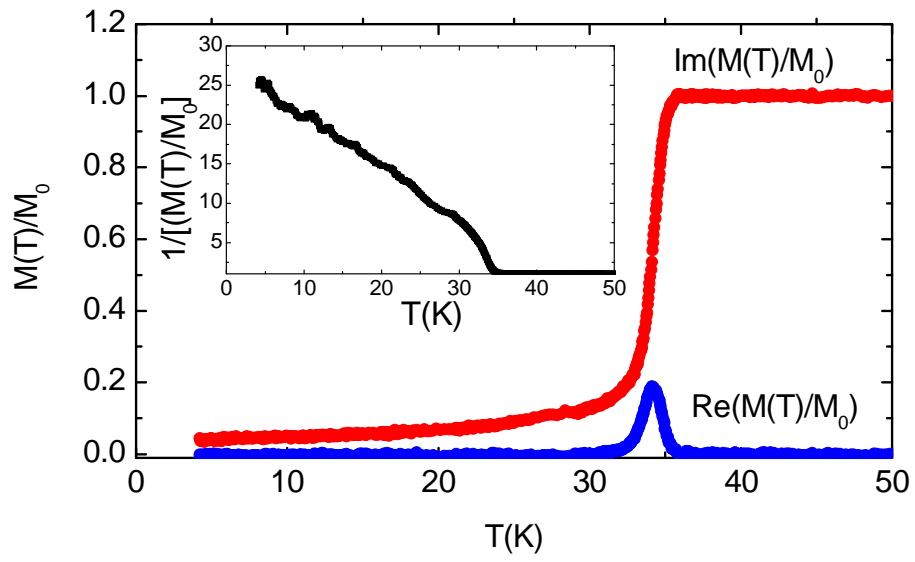


Figure 5

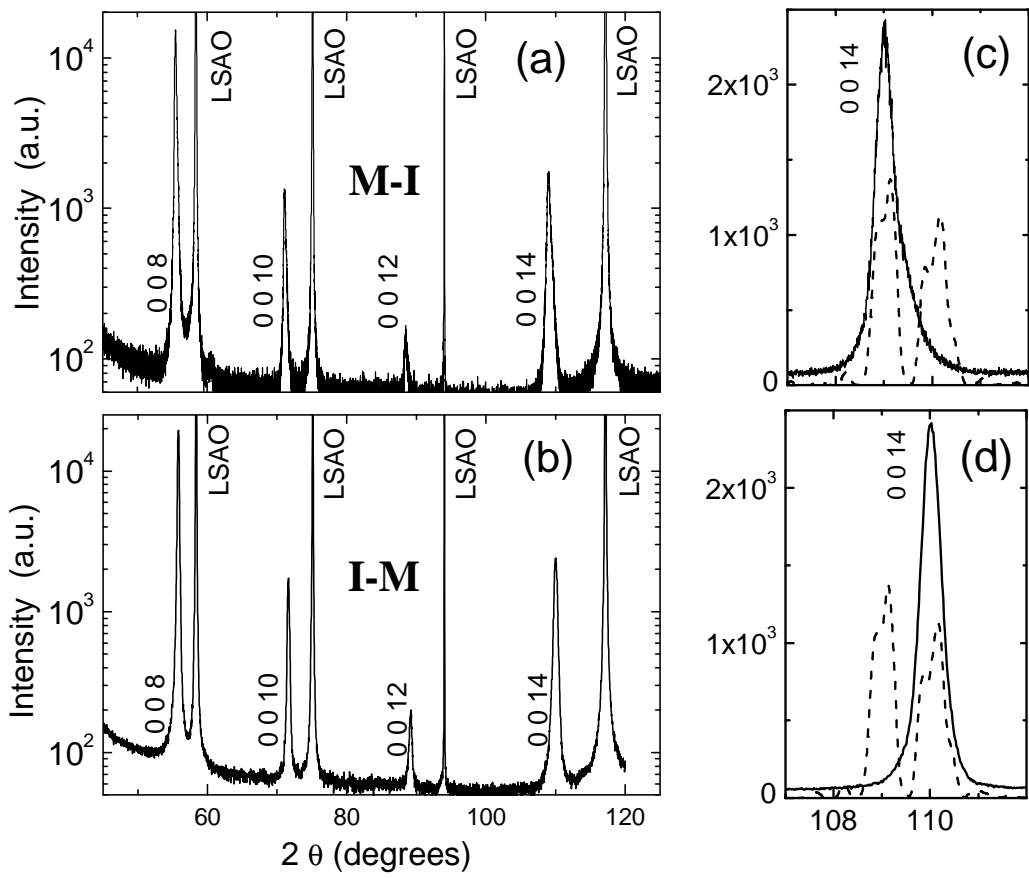


Figure 6

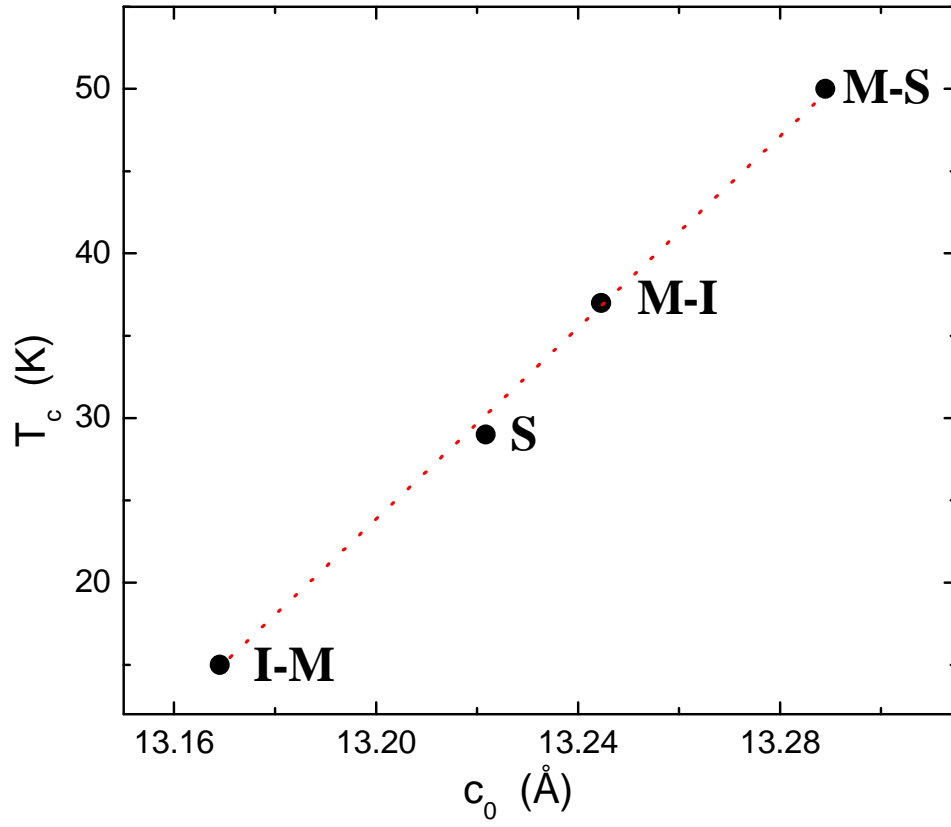


Figure 7